NeuroImage 283 (2023) 120403

Contents lists available at ScienceDirect

NeuroImage

journal homepage: www.elsevier.com/locate/ynimg

# The virtual aging brain: Causal inference supports interhemispheric dedifferentiation in healthy aging

Mario Lavanga [a,1], Johanna Stumme [b,c,1], Bahar Hazal Yalcinkaya [a], Jan Fousek [a], Christiane Jockwitz [b,c], Hiba Sheheitli [a], Nora Bittner [b,c], Meysam Hashemi [a], Spase Petkoski [a], Svenja Caspers [b,c,3], Viktor Jirsa [a,2,3,*]

[a] Institut de Neurosciences des Systèmes (INS), Inserm, Aix-Marseille University, Marseille 13005, France
[b] Institute of Neuroscience and Medicine (INM-1), Research Centre Jülich, Jülich, Germany
[c] Institute for Anatomy I, Medical Faculty & University Hospital Düsseldorf, Heinrich-Heine University Düsseldorf, Düsseldorf, Germany

ARTICLE INFO

*Keywords:*
White-matter degradation
Functional dedifferentiation
Functional connectivity
Structural connectivity
Aging
Cognitive decline

ABSTRACT

The mechanisms of cognitive decline and its variability during healthy aging are not fully understood, but have been associated with reorganization of white matter tracts and functional brain networks. Here, we built a brain network modeling framework to infer the causal link between structural connectivity and functional architecture and the consequent cognitive decline in aging. By applying in-silico interhemispheric degradation of structural connectivity, we reproduced the process of functional dedifferentiation during aging. Thereby, we found the global modulation of brain dynamics by structural connectivity to increase with age, which was steeper in older adults with poor cognitive performance. We validated our causal hypothesis via a deep-learning Bayesian approach. Our results might be the first mechanistic demonstration of dedifferentiation during aging leading to cognitive decline.

## 1. Introduction

Brain aging has been related to changes in cognitive functioning with substantial individual variability (Hedden and Gabrieli, 2004). So far, several biomarkers have been investigated to unravel underlying mechanisms that may account for this complex and highly variable relationship. Promising targets include grey matter atrophy as well as structural and functional brain reorganization (Reuter-Lorenz and Park, 2014). Brain structural atrophy, often assessed using measures, such as cortical thickness or grey matter volume, have been associated with a decline in a variety of cognitive functions, such as executive functions or memory (e.g. Reuter-Lorenz et al., 2021). Interestingly, older adults have been shown to differentially suffer from cognitive decline, despite the same levels of brain atrophy. Therefore, a vast amount of research started to focus on the age-related changes in the interaction of specific brain regions, i.e. cognitive brain networks. During the aging process, both, task-related functional activation patterns as well as task-independent functional connectivity (FC) hint at a functional brain reorganization, which is accompanied by structural brain reorganization, e.g. through a decline in structural connectivity (SC), i.e. the integrity of white-matter fibers connecting brain regions (Puxeddu et al., 2020), and regulatory changes in neuromodulation, such as dopamine (Berry et al., 2016). Structural and chemical changes are accompanied by functional reorganization in brain networks, i.e. functional connectivity (FC) of the brain regions (Stumme et al., 2020).

Based on these, contemporary aging theories (Festini et al., 2018; Reuter-Lorenz and Park, 2014) aim to link cognitive decline to age-related differences or changes in terms of brain structure, as well as structural and functional connectivity in older ages. For example, the 'Scaffolding Theory of Aging and Cognition' (STAC) (Reuter-Lorenz and Park, 2014) generally hypothesizes that the brain adapts to age-related brain atrophy and functional changes by recruiting alternative brain regions during task performance, thereby attempting to maintain cognitive functioning as stable as possible. Along a similar line of

* Corresponding author.
*E-mail address:* viktor.jirsa@univ-amu.fr (V. Jirsa).
[1] These authors contributed equally
[2] Lead contact
[3] Senior author

https://doi.org/10.1016/j.neuroimage.2023.120403
Received 2 November 2022; Received in revised form 20 September 2023; Accepted 5 October 2023
Available online 20 October 2023

research, several theories have emerged focusing on regional changes in brain function (Davis et al., 2008; Zhang et al. (2017) and related cognitive functioning during older ages, e.g. higher levels of activity in older than younger adults have been proposed to subserve maintenance of their performance, i.e. to compensate for age-related reorganization, e.g. structural deterioration. However, it has been suggested that at a certain point older adults' brains reach a point where a flexible increase in activation levels and therefore compensation is no longer possible and cognitive performance cannot be maintained stable (CRUNCH, Reuter-Lorenz and Cappell, 2008). Along this line of research, more bilateral patterns of functional brain activation have been observed in older adults during task performance (hemispheric asymmetry reduction in older adults, HAROLD; Cabeza, 2002; Cabeza et al., 2002), which might be interpreted as a compensatory mechanism to maintain cognitive function as stable as possible despite structural brain decline. Here, another explanation might be a process of functional dedifferentiation of brain regions, i.e. a loss of specificity of brain activation pattern, due to a decline in network efficiency.

The change in brain activation could be further extended to functional connectivity by e.g. Davis et al. (2012), who showed that for a bilateral task higher performing older adults recruit more bilateral regions of the prefrontal cortex than younger adults, resulting in higher FC that is supported by a higher callosal SC as compared to low performers. Furthermore, corpus callosum degeneration has been recently shown to impact $\boxed{\overset{\text{L}}{\text{SEP}}}$ the homotopic functional connectivity (Mollink et al., 2019; Roland et al., 2017) and the age prominence of interhemispheric structural degeneration (Puxeddu et al., 2020). Daselaar et al. (2015), on the other hand, links SC with higher activity during successful tasks in a "less wiring, more firing" hypothesis. Thus, SC and FC have been shown to be non-trivially linked during the aging process, and together impact cognitive performance.

However, despite the advent of imaging techniques and novel analysis methods, the assessment of SC and FC and their influence on cognitive function in the aging brain are correlative in nature, since we cannot manipulate one or the other. Hence, characterization of age-related differences in brain structure, function and cognition mainly relied on correlation analysis (Damoiseaux, 2017; Zimmermann et al., 2016), and in the cases when possible mechanisms were modeled (Petkoski et al., 2023), it relied on smaller cohorts. However, with recent studies suggesting corpus callosum degeneration to impact the homotopic functional connectivity (Mollink et al., 2019; Roland et al., 2017) and the age prominence of interhemispheric structural degeneration (Puxeddu et al., 2020; Petkoski et al., 2023), the causal influence of interhemispheric SC on functional dedifferentiation might be one mechanism contributing to the understanding of variability in cognitive decline. To disentangle these intertwined mechanisms and approach causality, we adapt a mechanistic causal inference framework, in which we balance the individual mechanistic contributions in a Virtual Aging Brain (VAB) model against empirical evidence in structural and functional brain imaging data and relate that to cognitive outcome.

As one mechanism characteristic of the aging brain, we here hypothesize that differences in structural interhemispheric connections contribute to variability and extent of FC. Moreover, age-related differences in FC have not only been observed in static FC (Stumme et al., 2020), but also in the reduction of its temporal variability, functional connectivity dynamics (FCD), reflecting the brain's capacity to switch among cognitive states (Battaglia et al., 2020; Petkoski et al. 2023). As a starting point for causal statements about the association between SC and FCD with variability in cognitive performance during the process of aging, we here focus on manipulating the coupling between interhemispheric SC and FC and assess its relation to cognitive performance. I.e., if we manipulate interhemispheric SC we expect the model to result in differences in FC and FCD. Further, we expect that manipulation of the global coupling between both will result in different brain working modes reflected in the model in line with aging theories, e.g. functional dedifferentiation or hemispheric asymmetry reduction, as well as cognitive outcomes. Furthermore, we compare the results from this simulated mechanistic framework against empirical imaging and cognitive data of a large population-based sample of older adults.

To this end, we developed personalized brain network models (BNMs), which integrate the individual SCs from the diffusion-weighted imaging (DWI) data of the participants of 1000BRAINS dataset ($n = 649$, age-range = [55–85] years, $n_{\text{females}} = 317$) (Caspers et al., 2014) to simulate functional data. Fig. 1 provides an overview of the general workflow. Each individual BNM is an ensemble of nodes, representing the different brain regions, constrained by the corresponding SC, which serves as the weighted adjacency matrix for the network. The neural activity of each node is obtained using an exact mean field model of the local neuronal population (Montbrió et al., 2015), exhibiting bistability of states of low and high firing rate (Fig. 1(A)). Brain's structure constraints the brain's capacity to generate certain dynamics characteristic of health and pathology (Fousek et al., 2022) and each BNM captures potential neuromodulation effects through a non-specific scaling of SC via the global network coupling parameter, $G$ (see Methods). Neural activity of each BNM was simulated in The Virtual Brain (TVB) platform (Sanz Leon et al., 2013) using the EBRAINS infrastructure on which TVB is intergated (Schirner et al., 2022). It generates time series for the mean neuronal firing rates from which corresponding BOLD signals were computed using the Windkessel model (Friston et al., 2000). To causally test the contributions of changes in white matter to functional reorganization, we conducted in-silico experiments in two scenarios. First, we extracted individual structural connectivity matrices ($SC_{emp}$) of the 1000BRAINS participants to design a BNM for each subject (Fig. 1(B)). Second, based on the declining age-trend of the interhemispheric connectivity strengths (Fig. 1(C)), we constrained BNMs via the connectomes of the 50 youngest subjects whose interhemispheric SC were homogeneously decreased from 0 % to 100 % ($\alpha$ parameter) by masking the antidiagonal edges of the SC matrix ($SC_\alpha$, an approach defined as "virtual aging", Fig. 1(D)). Note that this was the strongest trend observed in the empirical data, consistent with other studies (Petkoski et al., 2023). On the other hand, the overall decrease of the connectivity was statistically insignificant (Fig. S1(A)).

To benchmark the simulated dynamics with the empirical data, we computed a set of summary statistics for the corresponding resting-state functional magnetic resonance imaging: (i) the homotopic FC, defined as the average of the FC of same regions across hemispheres (Fig. 1(E)); (ii) the FCD variance, $\sigma^2_{full}$ (Fig. 1(E)); (iii) the FCD variance difference, obtained as the difference between the interhemispheric FCD variance, $\sigma^2_{inter}$, and the variance of full FCD, $\sigma^2_{full}$ (Fig. 1(E)) (see Methods). Homotopic FC (Stumme et al., 2020; Zuo et al., 2010) as well as the dynamical interplay between hemispheres (Escrichs et al., 2021; Xia et al., 2019) have been previously reported to be highly age-characteristic. To vary the hypothesized degree of neuromodulation, as represented by the global coupling parameter $G$, we swept $G$ in the range [1.5–3.2] and computed the associated FCD and its variance $\sigma^2_{full}$. Maximal values of FCD variance have been previously reported to be a proxy of brain fluidity (Rabuffo et al., 2021; Fousek et al., 2022), linked to cognitive flexibility (Naik et al., 2017; Senden et al., 2017), thus they would represent a potential target for optimization of potential compensatory processes of each BNM undergoing age-related changes. Hence, for each BNM we obtained a global $G$ as representative of the variation of the neuromodulatory drive that sets the SC tethering onto FC during aging and during interhemispheric SC deterioration.

## 2. Methods

### 2.1. Sample

Participants of the current study are based on the 1000BRAINS

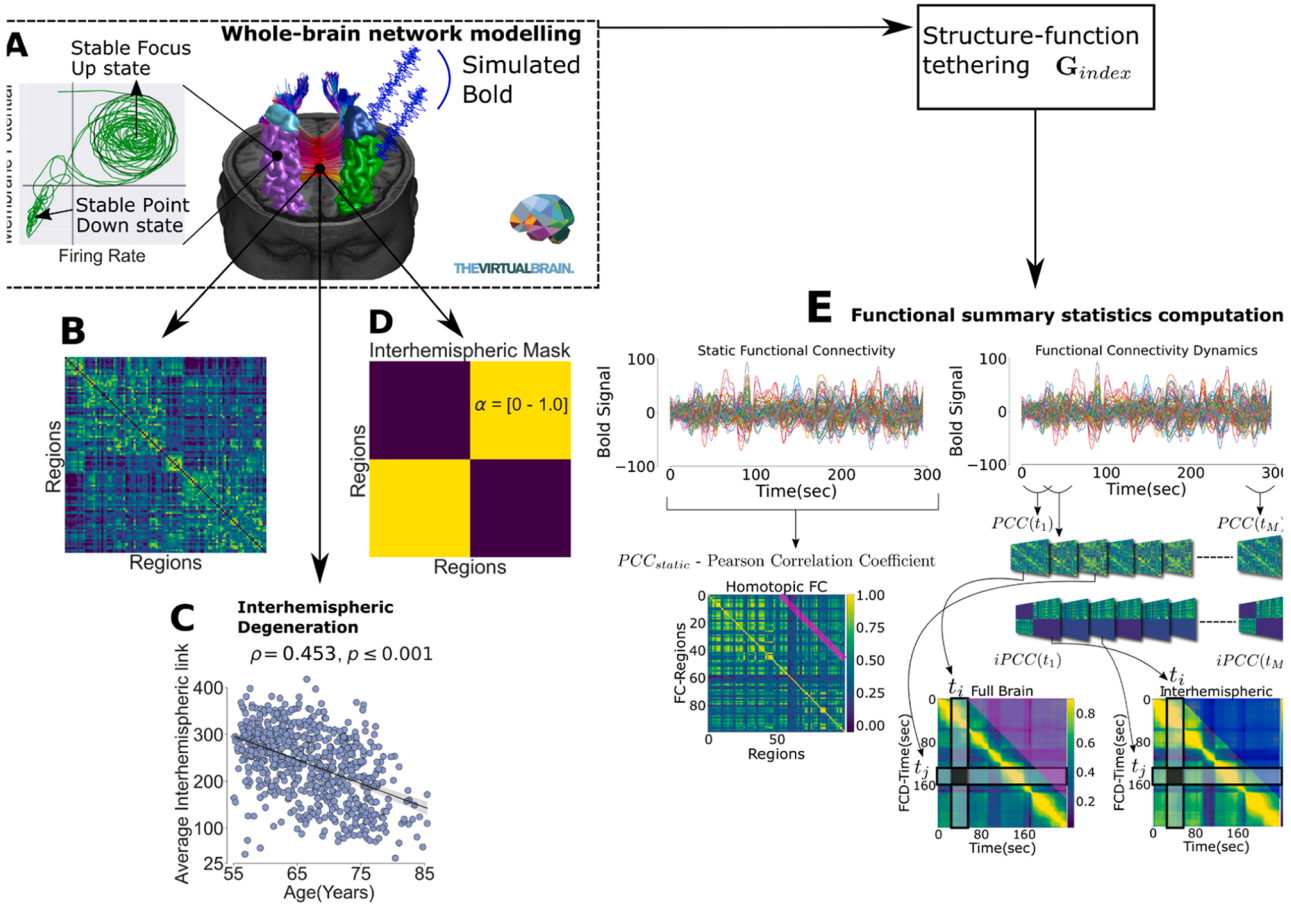


**Fig. 1.** Causal framework to link white matter degeneration with age-related functional changes. (A) Brain network models composed of neural mass models connected by the SC to simulate BOLD data. (B) Example of an empirical connectome of 1000BRAINS. (C) Interhemispheric SC decrease in the empirical data ($\rho = -45.3$ %, $p \leq 0.001$ corrected for sex and education). (D) Interhemispheric mask to artificially decrease SC of the 50 youngest subjects with various degrees of uniform changes (parameter $\alpha$ from 0 % to 100 %). (E) The computed summary statistics to benchmark and tune the VAB: the homotopic FC (magenta line in left panel), the FCD variance, variance of entries the magenta triangle (right panel), the FCD variance difference, which is the difference of the variance of entries between the blue and the magenta triangle (right panel). (For interpretation of the references to color in this figure legend, the reader is referred to the web version of this article).

project ($n = 1314$, 18–87 years, 582 females) (Caspers et al., 2014), a population-based study which was designed to analyze the normal aging process, i.e. the variability of brain structure, brain function and its relation to behavioral, environmental and genetic factors. 1000BRAINS is a subsample of the 10-year follow-up cohort of the Heinz Nixdorf Recall Study, an epidemiological population-based study that investigates risk factors for atherosclerosis, cardiovascular disease, cardiac infarction, and cardiac death, as well as the associated Multi-Generation Study. For 1000BRAINS, no exclusion criteria other than eligibility for MRI measurements (Caspers et al., 2014) were applied as the project aims to characterize aging at the general population level. Eligibility for MRI measurements included any history of neurosurgery, cardiac pacemakers, coronary artery stents, surgical implants or prostheses in head or trunk, tattoos or permanent make-up on the head. Participants gave written informed consent prior to inclusion in 1000BRAINS and MR imaging was only conducted as there were no dental implants found which could cause artifacts in the brain images and as participants did not experience claustrophobia. The study protocol of 1000BRAINS was approved by the Ethics Committee of the University of Essen, Germany. In the current work we focused on particularly older adults (above 55 years, $n = 970$), from which a total of 871 had functional scans available. 16 participants had to be excluded due to insufficient data quality. Of these 855 subjects, 718 also had diffusion data available, from which 649 were of good quality (see more details under Imaging). The current sample therewith comprises a total of $n = 649$ participants (age-range = [515.1–85.4] years, mean age = 67.2 years, $n_{females} = 317$).

To test how the causal link between white matter degeneration and functional changes could explain to interindividual variability of cognitive decline, we took advantage of the comprehensive neuropsychological assessment that was conducted within 1000BRAINS and included 16 cognitive performance tests into the current study (see Supplementary Table 2, for more details also see Caspers et al., 2014).

### 2.2. Imaging

All participants were scanned using a 3T Siemens Tim-TRIO MR scanner (32- channel head coil, Erlangen, Germany) located at the Forschungszentrum Jülich in Germany. Different imaging sequences, i.e. anatomical, diffusion and resting-state, were used in the current study to analyze the structural and functional connectivity linkage (for detailed description of the 1000BRAINS study protocol also see Caspers et al., 2014). For the anatomical image, a 3D high-resolution T1-weighted magnetization-prepared rapid acquisition gradient-echo (MPRAGE) anatomical scan (176 slices, slice thickness 1 mm, repetition time (TR) = 2250 ms, echo time (TE) = 3.03 ms, field of view (FoV) = 256 × 256 $mm^2$, flip angle = 9°, voxel resolution 1 × 1 × 1 $mm^3$) was acquired to perform a surface reconstruction. For structural connectivity, diffusion tensor images were acquired using the following parameters: a HARDI protocol with a subset (60 directions) EPI with TR = 6.3 s, TE = 81 ms, 7 b0-images (interleaved), producing 60 images with $b = 1000$ s/$mm^2$ and a voxel resolution of 2.4 × 2.4 × 2.4 $mm^3$; and a second HARDI subset (120 directions) EPI with TR = 8 s, TE = 112 ms, 13 b0-images

(interleaved), producing 120 images with $b = 2700$ s/mm$^2$ and a voxel resolution of $2.4 \times 2.4 \times 2.4$ mm$^3$. And lastly, for resting-state functional connectivity, we used a blood-oxygen level dependent (BOLD) gradient-echo planar imaging (EPI) sequence with 36 transversally oriented slices (slice thickness 3.1 mm, TR = 2200 ms, TE = 30 ms, FoV = $200 \times 200$ mm$^2$, voxel resolution $3.1 \times 3.1 \times 3.1$ mm$^3$), lasting for ~11 min and producing 300 volumes. Of note, during resting-state image acquisition, participants were instructed to keep their eyes closed, be relaxed, let their mind wander and not fall asleep, which was assured by post-scan debriefing.

#### 2.2.1. Structural image processing

Using the CAT12 toolbox implemented in SPM12 (Ashburner, 2009), we created tissue probability maps (TPM) for gray matter (GM), white matter (WM) as well as corticospinal fluid (CSF) from the participant's T1 data. These brain masks were used to optimally extract the brain from the T1 data by superimposing and thresholding them at 0.5 (small enclosed holes were filled). The T1 brain was bias field corrected, rigidly aligned to MNI152 template space and resampled to 1.25 mm isotropic voxel size. We corrected the diffusion MRI data for eddy current and motion artifacts including interpolation of slices with signal dropouts (Andersson et al., 2016). Subsequently, all diffusion data were visually controlled for ghosting, remaining signal dropouts or very noisy data and volumes or datasets that were considered as suboptimal were excluded from further analysis ($n = -69$). For dMRI - T1 alignment, the first b0 images from each dMRI data with b1000 and b2700 were extracted and rigidly aligned to T1 dataset using mutual information as cost function (Wells et al., 1996). Based on the estimated transforms, the dMRI data were transferred to the individual T1 space, separately for both b-values. Implicitly, the realignment resamples the data to 1.25 mm and rotates the b-vectors according to the corresponding transformations. As there are no field maps or b0 volumes with opposite EPI readout directions available in the current study, we computed Anisotropic Power Maps (APM) from the b2700 dMRI data in 1.25 mm space to account for susceptibility artifacts and optimize image registration (Dell'Acqua et al., 2014). APM contrasts are very similar to those of the T1 image and therefore provide an optimized base for image registration. Hence, APMs were used to compute the non-linear transformation from diffusion to anatomical space, thereby taking EPI induced distortions into account. These non-linear transformations were then used to transform the TPMs to diffusion space. Finally, the two datasets with b1000 and b2700 were merged into one single file and corrected for different echo times. This correction was computed by a voxelwise multiplication of the b2700 data with the ratio of the non-diffusion-weighted data respectively for the two datasets. Lastly, local modeling and probabilistic streamline tractography were performed using the MRtrix software package version 0.3.15 (Tournier et al., 2012). We computed the constrained spherical deconvolution (CSD) local model using multi-tissue CSD of multi-shell data (Jeurissen et al., 2014) with all shells and a maximal spherical harmonic order of 8. Ten million streamlines were computed with dynamic seeding in the gray-white matter interface for every subject using the probabilistic iFOD2 algorithm with a maximal length of 250 mm and a cut-off value at 0.06.

#### 2.2.2. Functional image processing

For each participant, the first four echo-planar imaging (EPI) volumes were discarded. To correct for head movement, a two-pass procedure was performed using affine registration: first, aligning all functional volumes to the participant's first image and second, to the mean image. Functional images were then spatially normalized to the MNI152 template using the "unified segmentation" approach by (Ashburner and Friston, 2005). This was preferred to normalization based on T1 weighted images as previous studies indicated increased registration accuracies (Calhoun et al., 2017; Dohmatob et al., 2018). Furthermore, to identify and remove motion-related independent components from functional MRI data, we applied the data-driven method ICA-based Automatic Removal of Motion Artifacts [ICA-AROMA (Pruim et al., 2015)]. According to previous suggestions indicating a combination of AROMA and global signal regression to minimize the relation between motion and resting-state Functional Connectivity (FC) (Parkes et al., 2018), we additionally performed global signal regression in the current study. Lastly, all rs-fMRI images were bandpass filtered (0.01–0.1 Hz). To assure data quality, we performed the established algorithm by (Afyouni and Nichols, 2018) on the preprocessed functional data of each participant, which generates $p$-values for spikes (DVARS) indicating volume-wise severe intensity dropouts. Participants with dropouts in more than 10 % of the 300 volumes were excluded ($n = -8$). Lastly, the "check sample homogeneity was performed using standard deviation across sample" function analysis provided by the CAT12 toolbox (Gaser et al., 2022) to check for potential misalignments. Participants detected as outlier were manually checked and excluded as the individual mean AROMA functional image did not align to the MNI152 template ($n = -8$).

#### 2.2.3. Parcellation

We parceled the whole-brain into 100 discrete and non-overlapping regions using the predefined 17-network parcellation scheme by Schaefer et al. (2018). The components provided by the 17-network parcellation can be allocated to the 7-network scheme, the latter being associated with seven distinct behavioral systems: visual, sensorimotor, limbic, frontoparietal, default-mode, dorsal and ventral-attention network (Schaefer et al., 2018).

#### 2.2.4. Structural connectome

For structural connectivity (SC), the parcellation template first had to be warped to individual diffusion space. This was done by combining the non-linear warps of the spatial T1 registration to MNI152 and the distortion correction with the APMs. Since streamlines are generated seeding from the gray-white matter interface and the predefined parcellation scheme only covers cortical gray matter, the template was expanded adding voxels towards the gray-white matter boundary so that all regions also include the seeding points. To increase the biological accuracy of SC, the SIFT-2 method was applied (Smith et al., 2015). Here, each streamline is weighted with an estimate of its effective cross-sectional area, so that the streamline density matches the white matter fiber density computed directly from the diffusion signal. Based on the estimated streamlines, we calculated the proportion of streamlines between regions (Puxeddu et al., 2020) resulting in a $100 \times 100$ adjacency matrix $w_{ij}$. The brain was then represented as a whole-brain connectome, in which the parcels are considered as nodes and the structural connections as edges $w_{ij}$ connecting node i and j. By means of CSD, $w_{ij}$ was computed as a density of streamlines between two regions by also correcting for the changing cross-sectional area. All 649 SC adjacency matrices (*Regions* $\times$ *Regions*) were normalized by the maximum of the entire 1000BD cohort.

#### 2.2.5. Functional connectome

For functional connectivity, we computed both, static FC as well as FC dynamics (FCD). For each of the 100 regions, mean fMRI time-series (BOLD signals) were extracted by averaging the functional activity of all voxels belonging to this region.

For static FC, the connectivity (edges) between regions (nodes) was estimated by correlating the mean time-series using the Pearson's correlation coefficient (static PCC or sPCC) resulting in a $100 \times 100$ FC matrix for each participant (Fig. 3). Noteworthily, to make our findings comparable to previous work and since negative connectivity values are discussed ambiguously (Stumme et al., 2020), we only considered the positive edges in the FC and set negative correlation values to zero.

FCD is the dynamic or time-variant representation of FC and reflects the fluctuation of the covariance matrix over time. FCD was quantified

by means of a sliding window Pearson correlation coefficient (dynamic PCC or dPCC). Following the procedure in Battaglia et al. (2020), we estimated the FC for a 40 s window with maximum overlap (slide step set to 1 sample) to obtain a stream or array of FC matrices that spread over time. The length of the window was set to 40 s as a trade-off between a lower sampling FC variability and a sufficient sensitivity to detect temporal FC transients (Lurie et al., 2020). The intrinsic dynamics of the stream was measured as the combinatorial similarity among the matrices of the stream of FCs (Fig. 2(E)). This match is defined as the Pearson correlation between FC at time or slice $t_1$ and FC at time or slice $t_2$ according to the formula

$$\begin{aligned} FCD(t_1,t_2) &= corr(UpperTri(dPCC(i,j,t_1)), UpperTri(dPCC(i,j,t_2))) \\ FCD(t_1,t_2) &= corr(UpperTri(FC(t_1)), UpperTri(FC(t_2))) \end{aligned} \quad (1)$$

which gives a *timeXtime* matrix known as the FCD Matrix. To assess whether the BOLD time series might have state transitions between high and low activity, we evaluated the switching behavior of BOLD as described in Rabuffo et al. (2021) by employing a compressed metric to assess this transitioning behavior. Therefore, we defined the switching index (SI) or FCD variance as the variance of the upper triangular part of the FCD matrix (Fig. 3) or its Frobenius Norm:

$$\sigma^2_{FCD,\ full} = \| \ Upper(FCD)_{full} \ \|^{\ 2} = \sum_{i>K}^{N} \sum_{j>i}^{N} \left| FCD(t_i,t_j) \right|^2 \quad (2)$$

The diagonal order K of the upper triangular matrix was set equal to dPCC window length (converted in samples) to correct for the overlap.

The empirical data analysis was repeated for windows of sizes [40, 50, 60, 80, 100, 150,180] seconds (Fig. S2), which all share the reported trends.

### 2.3. The virtual aging brain pipeline

For the investigation of the causal link between white matter degeneration and functional changes and its association with the heterogeneity of cognitive decline, we performed a two-fold analysis. In the first part, we addressed the questions whether realistic brain function can be modeled via a simulated SC decline. After we verified that the presence of a decline in the interhemispheric connectomes in empirical SC dataset, we designed virtual brains, brain network models constrained by the imaging data of SC, to predict brain function from the empirical SC dataset ($SC_{emp}$) as well as one virtually aged participant ($SC_{\alpha}$) (see Predicting functional connectivity: The Connectome-based Brain Network Model) and again, compared the derived (in-silico) functional data between each other as well as to the empirical (in-vivo) functional data (see Comparing estimated in-silico and in-vivo functional data) to ensure the SC changes of the virtual brains could reproduce age-related functional changes. Confident about the model performance, we then, in the second part, inspected the model derived output variable ($G$-modulation index) characterizing the tethering between SC and FC and related it to age, sex and cognitive performance (see SC-FC tethering and its association to age, cognitive performance and sex).

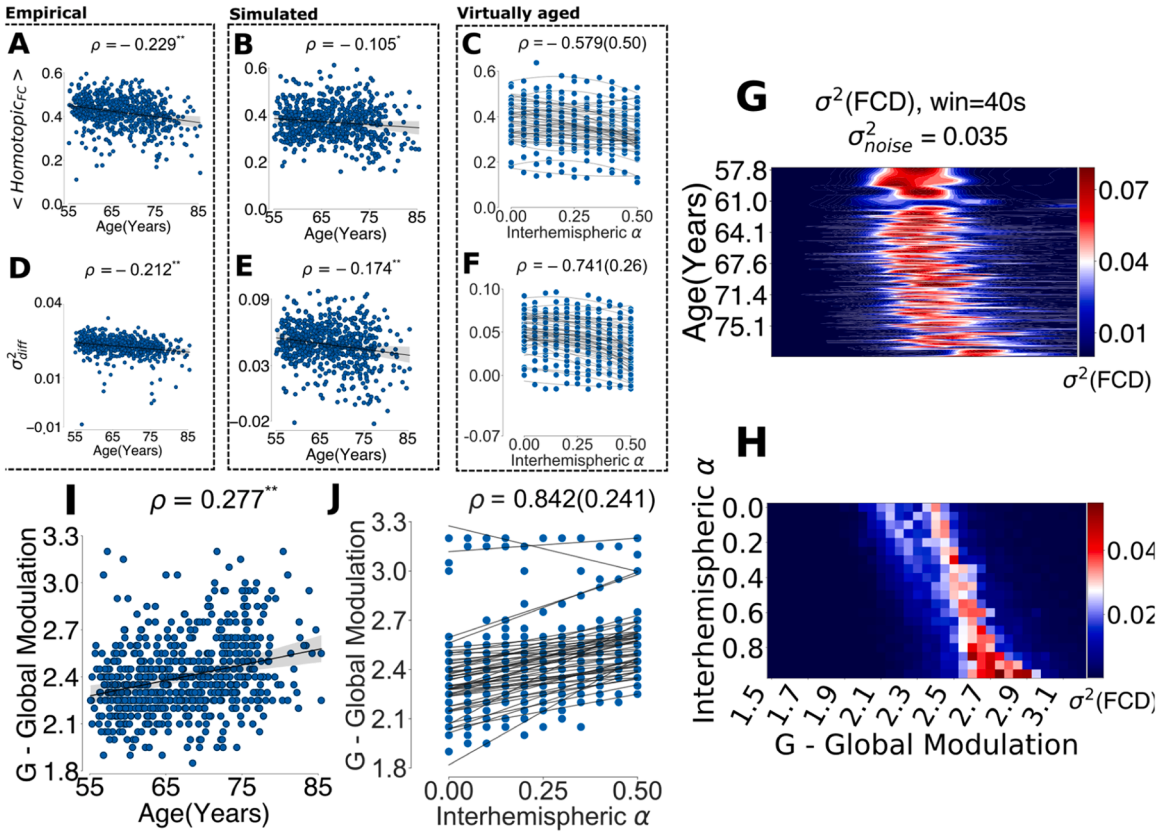


**Fig. 2.** Dedifferentiation occurs at both functional and global modulation levels. The trend for homotopic FC for the empirical (A), and the simulated (B) data in relation to age, and the virtually aged (C) data in relation to parameter $\alpha$ ($** \ p \leq 0.001$, $* \ p \leq 0.01$, (A-B) corrected for sex and education, (C) median ρ (interquartile range in parenthesis) over the virtually aged subjects, lines show regression curves of the trajectories for each of the virtually aged subjects). (D-E-F) FCD variance difference ($\sigma^2_{diff}$) in the same three datasets ((D-E) corrected for sex and education, (F) Median(IQR)). (G) Heatmap of the simulated FCD variance $\sigma^2_{full}$ for the entire 1000BRAINS dataset along two dimensions: $G$ (it has the same axes as the plot in H) and the age of each SC, with the noise variance fixed at $\sigma^2_{noise} = 0.035$. (H) Heatmap of FCD variance $\sigma^2_{full}$ for a virtually aged target subject along two dimensions: $G$ and $\alpha$. (I-J) The G associated to maximum of FCD variance and its trend with age ($** \ p \leq 0.001$, corrected for sex and education) and $\alpha$ (median (IQR)).

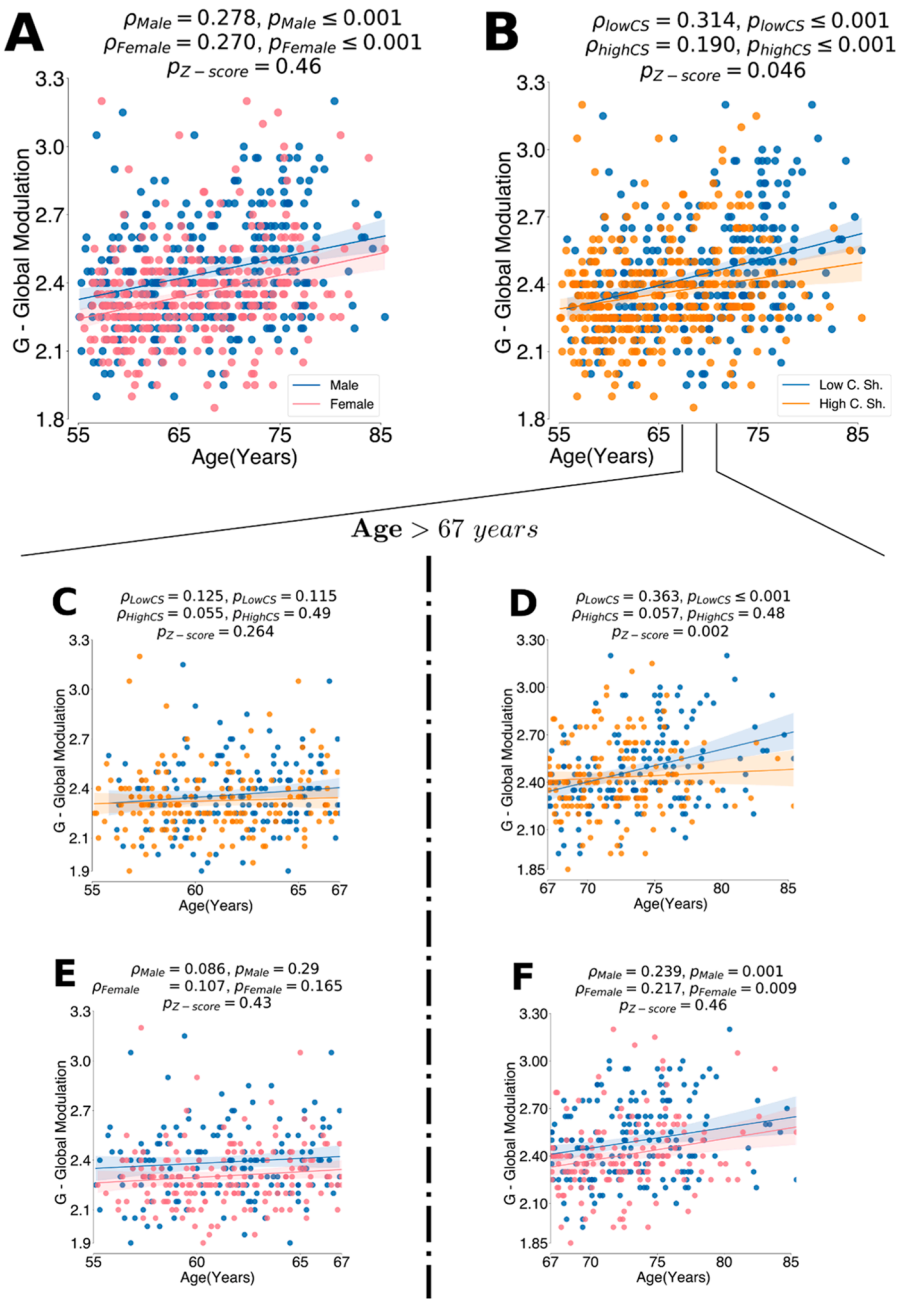


**Fig. 3.** Global modulation age-increase is more prominent in low cognitive performers. (A) The trend of G split by sex: women (pink) and men (blue) (Fisher's Z: $p = 0.46$,$\rho$ corrected for sex and education) (B). The aging G trend split by concept shifting: low performers (blue) and high performers (orange) (Fisher's-Z: $p = 0.046$,$\rho$ corrected for sex and education). (C-D) The same trend in (B) split by the median age 67 years to trends for the younger subjects and older ones (Fisher's-Z: $p = 0.264$ and $p = 0.002$, respectively). (E-F) The same trend in (A) split by the median age 67 years for the younger subjects and older ones (Fisher's-Z: $p = 0.43$ and $p = 0.46$, respectively). (For interpretation of the references to color in this figure legend, the reader is referred to the web version of this article).

*2.3.1. Predicting functional connectivity: the connectome-based brain network model*

The approach to virtually age a structural connectome provides the basis to test whether a specific modification in SC affects brain function in a causal sense. Therefore, as a preliminary investigation, we inspected the empirical SC datasets with regards to age and specifically tested whether the previously reported strong age-related interhemispheric SC decline (Puxeddu et al., 2020; Roland et al., 2017) is also applicable to the current dataset of older adults (see Fig. 2).

Furthermore, we performed a virtual aging process on the 50 youngest participants (mean age, age-range) by homogeneously decreasing the interhemispheric connections. In particular, we applied a mask on the empirical connectome $W_0$ as follows:

$$W = W_0 - \alpha M_{inter} * W_0 \tag{3}$$

where $M_{inter}$ is the antidiagonal mask, $\alpha$ is the normalized intensity of decrease and * represents an element-wise product (see Fig. 2). The $\alpha$ parameter was spanned in the range [0–1] with sampling interval 0.05 resulting in 20 virtually aged structural connectomes per subject (SC).

The $\alpha$-masking approach was used to assess the direct impact of the simulated interhemispheric SC decrease on the simulated functional data. To assess the effect of age-related interhemispheric SC degeneration on the brain dynamics in a causal sense, we applied the brain network model in two scenarios. We simulated resting-state activity via

virtual brains that couples neural mass (NM) models described in (Montbrió et al., 2015) through the weighted edges in the SC matrix of all participants ($n = 649$) (Fig. 2(A)) or via the virtually-aged or $\alpha$-masked matrices of the 50 youngest subjects (Fig. 2(B)). The nodal dynamics is a mean-field representation of an ensemble of infinite all-to-all connected quadratic-integrate-and-fire (QIF) neurons at the thermodynamic limit. Following (Montbrió et al., 2015; Rabuffo et al., 2021) and assuming that input currents to the mass system were distributed according to a Lorentzian distribution, the dynamics of each region were given by the following equations:

$$\begin{aligned} \dot{r_i}(t) &= \frac{\Delta}{\pi} + 2r_iV_i(t), \\ \dot{V_i}(t) &= V_i^2(t) + \eta + Jr_i(t) - \pi^2 r_i^2(t) + I_i(t), \end{aligned} \tag{4}$$

where the variable $r_i(t)$ is the population firing rate, while $V_i(t)$ is the average membrane potential of the mass. The parameter $J$ represents the average synaptic weight, while the parameter $\eta$ and $\Delta$ represent the average excitability of the mass neurons and the heterogeneous noise spread, respectively. These two parameters represent the center and the half width of the Lorentzian distribution of the input currents. The values of these three parameters were set to $J = 14.5$, $\eta = -4.6$, $\Delta = 0.7$ in order to obtain a bistable regime, meaning a down-state fixed point and an up-state stable focus in the phase space (Rabuffo et al., 2021). The bistability is a fundamental property to ensure a switching behavior in the data, that has been considered representative of realistic dynamics of real data (Rabuffo et al., 2021; Fousek et al., 2022). The dynamics of a node can arise by the oscillation between these two points (the down-state and the up-state) in the phase space thanks to current $I_i(t)$. We could then model a brain network model by $I_i(t)$ with:

$$I_i(t) = G\sum_{j\neq i}^{N} w_{ij}\, r_j\,(t-\tau_{ij}) + \xi_i \tag{5}$$

and obtaining the coupled differential equation:

$$\dot{V}_i(t) = V_i^2(t) + \eta + Jr_i(t) - \pi^2 r_i^2(t) + G\sum_{j\neq i}^{N} w_{ij}\, r_j\,(t) + \xi_i \tag{6}$$

where $r_j\,(t)$ is the firing rate coming from other regions weighted by the structural connectivity edges $w_{ij}$. The variable $\xi_i$ represents the noise that models stochastic external factors and allows the region i to oscillate between the two states. The parameter $G$ is the global parameter that modulates the overall impact of SC on the state dynamics of each region and the $\xi_i$ is the noise variable that ensures the oscillations between the up-state and down-state and is distributed according to a Gaussian distribution with a variance set to $\sigma$. Note that the model neglects the axonal delays assuming instantaneous synaptic couplings between the brain regions. The reason is that the model's dynamics is shaped by the neuronal cascades (Rabuffo et al., 2021) that are much slower than the delays, which in the case of diffusive couplings can constrain the faster neuronal oscillations (Petkoski and Jirsa, 2019) and activation patterns (Petkoski and Jirsa, 2022).

For each connectome, the brain network model was fitted by optimizing parameters $G$ modulation index and noise variance $\sigma^2$ to maximize the SI or $\sigma^2_{FCD,\ full}$ of the simulated BOLD data (see Fig. 3). SI is an indicator for the metastability or switching behavior of functional brain networks and can be used as a measurement for the realistic evaluation of brain function (Naik et al., 2017; Rabuffo et al., 2021). In fact, previous results indicate simulated data which was created by the enhancement of a metastable or switching behavior and tuning model parameters have been considered to provide more realistic dynamics than those minimizing the distance between the empirical FC and the simulated one (Senden et al., 2017). The capacity to replicate empirical data does not only entail the ability to reproduce a specific property of the functional data, but reproduce a wider range of features or summary statistics, such as static FC and other FCD properties. Specifically, for each dataset we conducted a parameter sweep or grid search for the global parameter in the range $G = [1.5 - 3.2]$ with sampling interval $\Delta G = 0.05$ and the noise variance in the range $\sigma^2 = [0.01 - 0.05]$ with $\Delta\,\sigma^2 = 0.01$ to determine the optimal couple $(G, \sigma^2)$ for which SI is maximal. The direct numerical integration for the nodal equations (2) was performed via Heun-stochastic integration implemented in the Virtual brain open-source code. For each region, we integrated the equations with variable time steps (from 0.005 ms to 0.0005 ms) for 5 min and we downsampled the variables $r_i(t), V_i(t)$ to the sampling frequency $fs = 100$ Hz. The time step was variable to adapt the integration process and avoid numerical errors or instabilities and the neural mass field was filtered via the Balloon-Windkessel model (Friston et al., 2000) to emulate fMRI time series with repetition time TR set to 2000 ms.

For each model fit (the 649 empirical and $20 \times 50 = 1000$ virtually aged connectomes), we obtained a $G$ modulation index which is representative of how much the SC influences the brain dynamics. Before investigating if the SC-FC causal link was related to behavioral factors such as age, sex and cognitive performance, we compared the in-silico brain dynamics to in-vivo data assuring that a variety of dynamic and static properties of functional covariates are indeed realistic.

### 2.3.2. Comparing estimated in-silico and in-vivo functional data

To ensure that the maximization of the SI indeed provides realistic functional dynamics, we estimated and compared a set of dynamic and static FC properties in the empirical data, in the age-simulated data and in the alpha-simulated data (or virtually aged data). In particular, we focused on functional biomarkers that have previously been shown to be biologically related to white-matter degeneration at microstructure level and to the cross-hemispheric SC topology (Mollink et al., 2019; Roland et al., 2017).

Specifically, we computed the average homotopic FC strength, the FCD variance difference, the standard deviation of the interhemispheric FC stream. The average homotopic FC strength is defined as the average sum of the specular interhemispheric connections, as follows:

$$\langle Homotopic_{FC}\rangle = \frac{1}{N/2}\sum_{i,j=i+N/2}^{N/2} FC(i,j) \tag{7}$$

where the averaged $FC(i,j)$ entries represent the element of order $K = \frac{N}{2}$. This definition is derived by the microstructure-function investigation by Mollink et al. (2019). We derived both the average of all homotopic edges or the average of edges connecting homotopic regions within a certain rsFC network. To extend the SI towards an interhemispheric topology, we computed the FCD variance difference as the difference between the SI of interhemispheric FCD matrix and the SI of the full FCD matrix, as follows:

$$\sigma^2_{diff} = \sigma^2_{FCD,\ inter} - \sigma^2_{FCD,\ full} \tag{8}$$

The $\sigma^2_{FCD,\ inter}$ was computed by considering only the interhemispheric edges of dPCC in each window and therefore in the similarity computation (see Fig. 3). The variance is then obtained as the Frobenius norm of the upper triangular part of the interhemispheric FCD matrix:

$$\sigma^2_{FCD,\ inter} = \|\ Upper(FCD)_{inter}\ \|_2^2 = \sum_{i>K}^{N}\sum_{j>i}^{N} \left|FCD_{inter}(t_i,t_j)\right|^2 \tag{9}$$

Similarly, one can compute the standard deviation of the interhemispheric FC stream as the variability of the interhemispheric FC edges of the FC matrix stream obtained with the windowing scheme. By unraveling the FC matrix in each slice, we obtained a vector 'FC edges' for each time point or *edges* $\times$ *time* matrix. We derived the standard deviation of all interhemispheric edges' time-courses as a representative index of the connectivity oscillations across hemispheres or the stability

of the metaconnectivity (Faskowitz et al., 2020).

#### 2.3.3. Simulation-based inference

The global modulation parameter $G$ of the brain network model was also estimated by simulated-based inference (SBI) framework tailored to Bayes rule in order to retrieve the model parameter space compatible with the empirical data (Cranmer et al., 2020; Gonçalves et al., 2020; Hashemi et al., 2023). Statistical inference consists of the automatic identification of possible parameters $\theta$ via the likelihood function $p(X|\theta)$, which quantifies the probability that a given set $\theta$ generates the vector of raw data or low-dimensional data features $X$. The Bayesian estimation consists in $p(\theta|X) = p(X|\theta)\, p(\theta)$, where $p(\theta|X)$ is the posterior that quantifies the probabilistic consistency between the selected parameter space and fitted empirical data (Hashemi et al., 2020; Hashemi et al., 2021). In order to evaluate the likelihood function for a high-dimensional mechanistic model such as the brain network model in this study, we used the sequential neural posterior estimation (SNPE) to approximate the distribution $p(X|\theta)$ with a flexible neural density estimation trained on low-dimensional data features (Gonçalves et al., 2020; Hashemi et al., 2023). SNPE is based on the training of a deep neural network, which allows to directly approximate all posteriors from ad-hoc data features, where the calculation of likelihood function is analytically or computationally intractable. Based on a "budget" of simulations obtained by a mechanistic model and a specific set of (low-dimensional) summary statistics derived from the generated data, the weights of the network are optimized through loss minimization using masked autoregressive flow (MAF; Papamakarios et al., 2017), bypassing the need for the highly computational intensive Markov chain Monte Carlo sampling (Gonçalves et al., 2020). Therefore, this approach is considered as a simulation-based inference approach that is amortized: after an upfront computational cost during the simulation and training steps, a new data set of the subject can be fitted efficiently by a single forward pass of the empirical data through the neural network, without the need for additional simulations during the inference step, thus reducing computational overhead (Gonçalves et al., 2020; Hashemi et al., 2023). In this study, a "budget" of 2000 simulations was obtained by the model in Eq. (2) and the network was trained on a matrix $X$, which contained the following three features or summary data for each simulation: average homotopic FC strength, the difference between the whole-brain FCD and the interhemispheric FCD, the standard deviation of the interhemispheric FC stream. The simulations were performed with a $G$ that was distributed according to a uniform prior (truncated between 1.5 and 3.2), such that the final posterior estimation resulted in: $p(G_{SBI}|X_{empirical}) = p(X_{simulated}|G_{SBI})$. As highlighted by the formula, the SNPE was repeated on each subject, trained on the simulated data and the final estimation of $G$ was obtained by maximizing the log likelihood of the features of the empirical BOLD data under the model. The SNPE provides the probabilistic statistical relation between G and the empirical data, and the final estimate of $G_{SBI}$ was considered as the maximum value of the estimated posterior distribution. For each individual SBI, the noise variance was set to the optimized value obtained via the parameter sweep. The quality of SNPE was evaluated as the Pearson correlation between $G_{SBI}$ and $G_{Sweep}$ as well as the trend of $G_{SBI}$ with age. We also checked the uncertainty of the estimations encoded in posterior distribution for each subject. The SNPE estimation was also validated using the in-silico data generated by TVB for one subject, as the estimated posterior distributions accurately encompass the ground truth values used in the simulation (see Fig. S3 in the supplements).

### 2.4. Quantification and statistical analysis

To test whether we could actually reproduce the dynamical and statical properties of FC, we estimated linear trends of the homotopic FC and FCD variance difference features in the functional empirical data, the age-simulated data and the alpha-simulated data. Specifically, we performed Pearson correlations between the functional summary statistics and age or the alpha masking variable, respectively.

The model-derived tethering between SC and FC ($G$ modulation index) was then statistically related to both demographic and behavioral factors. First, we performed an ANCOVA indicating whether the $G$ index is overall age- or sex-related (corrected for education). Furthermore, to analyze age-related trajectories of the SC-FC linkage, we performed partial correlations between the $G$ modulation index and age (corrected for sex and education). This was repeated after stratifying the group by sex, and the partial correlations (corrected for education) were statistically compared (Fishers-Z) indicating whether age-related $G$ modulation index changes are different in males as compared to females. Lastly, we performed a Pearson's correlation to test the relation between the $G$ modulation index of the virtually aged dataset and the alpha-variable.

According to various aging theories (Festini et al., 2018; Reuter-Lorenz and Park, 2014), changes in the SC-FC tethering might explain the variability of cognitive performance during the aging process. To test this hypothesis, we performed ordinary-least squares (OLS) multivariate regressions for each of the 16 cognitive scores, testing the relation between the cognitive performance and the G-coupling index, while correcting for age, sex and education. We specified the model as:

$$Cognitive\ Score = \beta_0 + \beta_G\, G + \beta_{age}\, age + \beta_{sex} sex + \beta_{edu} edu + \in \quad (10)$$

Here, results were considered significant at $p \leq 0.05$, Bonferroni corrected for the number of performed models ($n = 16$ cognitive scores, $p_{corr} = p_\beta/16$).

Moreover, for cognitive performance scores showing a significant relation to the $G$ modulation index, we were interested whether the strength of performance determines a different age-related trajectory in the $G$ index. Specifically, we split the whole group by the performance median into a low performing (LP) and a high performing group (HP) and tested whether the $G$ modulation index is significantly different between groups (ANCOVA corrected for sex, education and age). We also calculated partial correlations between age and the $G$ modulation index (corrected for sex and education) and compared these between groups (Fishers-Z). Post-hoc, based on a depicted non-linear trend of the correlation between age and the $G$ modulation index in particularly the low performing subjects, we split the groups by the median age (67 years) into a younger and older group. Partial correlations between age and the $G$ modulation index (corrected for sex and education) were repeated group-wise (for low and high performers in young and older subjects) and subsequently compared between low and high performing groups using Fishers-Z (see Fig. 4).

## 3. Results

### 3.1. The virtual aging brain model replicates age-related functional changes

The summary statistics of the simulated data of the BNMs constrained by the individual $SC_{emp}$ (Fig. 2(B), (E)) display a declining age-trend conforming to the empirical data (Fig. 2(A), (D)), which indicates a fading interhemispheric communication and dynamical variability. Similarly, the summary statistics emerging from the virtually aged BNMs (constrained by $SC_\alpha$) display declining trends with increasing $\alpha$, similarly to the empirical dataset as well as the BNMs constrained by the $SC_{emp}$.

We also investigated the landscape of brain fluidity ($\sigma^2_{full}$) for the different $G$ values of the parameter sweep and for different age of the $SC_{emp}$ (Fig. 2(G)), as well as for different $\alpha$ values applied to a sample target out of the 50 subjects (Fig. 2(H), see the remaining 49 subjects in Fig. S2). The red stripes display the peak of FCD variance at which the value of $G$ of each BNM was tuned, highlighting that age-related differences in SC (empirically as well as virtually) have an increasing modulation effect on the respective functional architecture. This

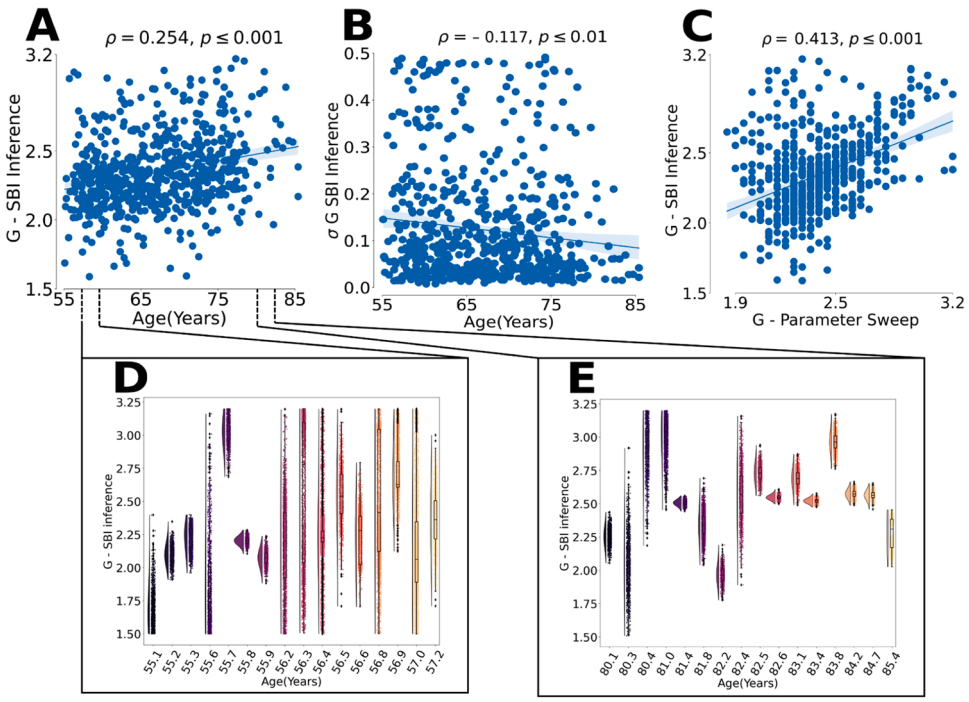


**Fig. 4.** Bayesian Inference confirms the age-increase of the global modulation. (A) The maximum posterior of global modulation $G$ obtained by SBI with age similarly to Fig. 3(I). (B) The standard deviation of the posterior distribution of $G$ obtained by SBI. (C) The correlation between $G$ modulation index obtained with SBI and the $G$ obtained by parameter sweep. (D) The posterior distribution of $G$ obtained with SBI for the subjects in the lifespan [55–57] years. (E) The posterior distribution of $G$ obtained with SBI for the subjects in the lifespan [80–85] years.

becomes clearer in plots I and H, where the values of $G$ for highest fluidity are shown for the simulated and virtually-aged subjects respectively. At the same time, the chosen values of G are also inversely correlated with the mean interhemispheric connectivity ($p < 0.001$, rho $= -0.59$), Fig. S1(B), but insignificantly correlated with the mean overall connectivity ($p = 0.88$, rho $= 0.006$), Fig. S1(C). A significance of the latter relationship would have been expected for a system in a linear working regime.

In addition, the independent analysis that we performed shows that the correlation between the $G$ parameter and age does not survive when we control for the decrease in interhemispheric connectivity ($p = 0.48$, rho $= 0.028$), supporting the compensatory effect that $G$ plays in regard to the white-matter loss.

### 3.2. Structural connectivity neuromodulation increase is related to higher cognitive decline

Within this framework, the heterogeneity of cognitive decline can be related to the trajectory of the modulation $G$ (Reuter-Lorenz and Park, 2014) via ordinary least squares (OLS) regression corrected by age, sex and education. Neuromodulation $G$ was significantly related with age and sex (ANCOVA corrected for education, sex: $p \leq 0.001$, age: $p \leq 0.001$, see Methods), with increasing age associated with higher global $G$ ($\rho = 27.71$ %, $p \leq 0.001$, corrected for sex and education, Fig. 3(I)). Importantly, the $G$ values obtained from $SC_\alpha$ also revealed a robust increase of neuromodulation as a function of $\alpha$, the virtual proxy for age in the VAB ($\rho = 89.97$ % (9.8 %), median (IQR), Fig. 2(J)). It is worth noting here that the age × sex interaction is not significant for $G$ ($t$-test $p = 0.868$).

Females were found to exhibit significantly lower structure-function modulation as compared to males (Fig. S4(A) for all the subjects, and Fig. S4(B), (C) respectively for the younger and the older portion separately), with a constant difference across age as both sexes showed comparable correlations between $G$ and age (Fig. 3(A)). Moreover, $G$ was significantly related to the performance in executive function, namely concept shifting (OLS: $\beta_G = -19.94$, $p_G = 0.043$, see Methods and Supplementary Table 1), with a higher $G$ associated with lower performance.

Splitting the subjects by the performance median into low (LP, $n = 327$) and high (HP, $n = 322$) performing subgroups revealed that LP are not only associated with a significantly higher $G$ as compared to HP (ANCOVA: $p = 0.019$), but also presents a stronger age-related increase of $G$ (Fisher's-Z: $p = 0.046$, Fig. 3(B)). We additionally split the subjects by age into older and younger age groups (cut by median = 67 years), which independently significant show differences in the slopes of with age (Fig. S5). In older LP subjects, the age-related trajectory of $G$ showed a stronger increase as compared to HP subjects (Fisher's-Z: $p = 0.002$, Fig. 3(D)), while the younger LP did not present a different trajectory from the HP group (Fisher's-Z: $p = 0.264$, Fig. 3(C)). Notably, $G$ was significantly related to verbal memory ($\beta_G = -4.94$, $p_G = 0.044$, see Methods and Supplementary Table 1). This, however, was not accompanied by a stronger correlation between performance and $G$ in LP, neither in the older age group nor in the entire cohort.

### 3.3. Simulation-based inference confirms the increase of the structural connectivity neuromodulation

Individual values of the neuromodulation parameter, $G$, were then casually validated for each BNM with a Simulation-based Inference (SBI; Cranmer et al., 2020) framework. This was done using the sequential neural posterior estimation (SNPE) method (Gonçalves et al., 2020; Hashemi et al., 2023), and a set of summary statistics of the empirical data, including homotopic FC, the FCD $\sigma^2_{diff}$, and the standard deviation of the interhemispheric FC stream (see Methods). The obtained values of $G$ via SBI showed a rising trend with increasing age (Fig. 4(A)), in line with the results obtained with the parameter sweep (Fig. 4(C)), which indicate an increase in global neuromodulation and, in general, in model evidence in association with the age-related decreasing interhemispheric structural connectivity. The variance in the parameter posterior distribution is quite high in both cases, indicating a high degree of

degeneracy of the model for the chosen data-features and parameters, and this seems to decrease with aging (Fig. 4(B)). A possible explanation is that younger subjects have higher resilience because larger ranges of the parameters can cause the desired dynamics/function. For better illustration, we also obtained the posterior distribution of the modulation $G$ as a further index of the estimation uncertainty and shift of model evidence with increasing age (Fig. 4(D) and (F), see Methods).

It is worth noting that there is a lot of variance in $G$ values obtained with SBI for each value from the sweep, Fig. 4(C). However, this is not surprising given that SBI is performed for a summary statistics of only three metrics, which besides the fluidity of FCD that is used for the sweep, also includes both metrics that showed the strongest predictive power for the age, that is the homotopic FC and the standard deviation of the interhemispheric FC stream.

## 4. Discussion

The present study developed individual brain network models (BNMs), which integrate the individual interhemispheric SCs (weighted fiber-bundle capacities derived from diffusion-weighted imaging data) of older adults to simulate functional BOLD time series. Through scaling of SC, i.e. by manipulating the global network coupling parameter $G$, each BNM displays individual variations of modulation of these time series, which were benchmarked with the homotopic FC, as well as the (interhemispheric) FCD variance.

Thus, in this particular study we focused on the modulatory effect of the interhemispheric SC onto the functional time series, and in particular their co-variance. We hypothesized that experimentally decreasing the interhemispheric SC ($\alpha$ parameter) would mimic one mechanism of the structural aging process in the brain (i.e. "virtual aging") and consequently be associated with FCD reductions.

Neurocognitive theories of aging argue that functional changes related to structural deterioration are either beneficial or detrimental and mediate cognitive decline (Festini et al., 2018; Reuter-Lorenz and Park, 2014). One claim in these theories is that the brain must adopt alternative signaling pathways to maintain cognitive function and preserve information exchange (Naik et al., 2017). The VAB framework aims to bridge the gap between mechanisms underlying healthy aging: in the current study we focus on structural connectivity degradation and adaptation of the system state through the structure-function tethering that is linked to neuromodulation, and their competing effects on neurofunctional reorganization and subsequent changes on cognition. Scaffolding and functional differentiation are normal processes present across the lifespan that involve use and development of complementary, alternative neural circuits to achieve a particular cognitive goal (Reuter-Lorenz and Park, 2014). This understanding of dedifferentiation is related to task-based data but not limited to it. For example, neural structures become less functionally differentiated and specialized with age during visual tasks (Park et al., 2004), but also during rest when weaker functional connectivity within resting state networks and stronger functional interaction between these networks have been shown cross-sectionally (Stumme et al., 2020) and longitudinally (Malagurski et al., 2020). Hence, the behavioral performance in older adults is often hypothesized to depend on keeping some quantity invariant through compensation in another. Preservation of neuronal synchrony in aging through enhancing inter-areal coupling has been suggested as one such example (Pathak et al., 2022). Here, the functional feature that is kept invariant is the maximal fluidity, and we demonstrate that the increase of global coupling is necessary to achieve this, as it was also shown to be necessary to achieve the best fit of the aging-related fluidity changes (Petkoski et al., 2023). The compensation that we are discussing is perfectly plausible from the dynamical viewpoint, but it is still unknown which biophysical mechanism could be responsible for the shift in the global coupling. $G$ is a purely phenomenological parameter, which has been shown to be important in setting the working point in the case of epilepsy (Courtiol et al., 2020). Most likely, it is linked to the regulatory changes in neuromodulation that are missing in our model, particularly the aging-related increase of dopamine synthesis capacity (Berry et al., 2016).

As a result of our framework, the simulated functional data of the BNMs, constrained by the empirical SC, displayed a declining age-trend in FC comparable to the empirical data: i.e. we observed lower homotopic FC with older age. When constraining the BNMs by homogeneously manipulating SC, i.e. when we decreased the interhemispheric SC, we also observed declining trends in FCD variance with increasing $\alpha$, again in line with the empirical data and the empirically constrained BNMs. Firstly, this mechanistically supports the hypothesis that interhemispheric SC serves as a basis for homotopic FC (Mollink et al., 2019; Roland et al., 2017). Secondly, FCD variance has previously been reported to be a proxy of brain fluidity, which has been linked to cognitive flexibility (Naik et al., 2017; Rabuffo et al., 2021; Senden et al., 2017). In our virtual approach, we hypothesize that the brain tries to maximize its fluidity (i.e. FCD variance as a proxy for it). Consequently, in the model we set the working point of $G$ such that fluidity is maximized.

Taken together, when we observe the lower FCD variance with lower (empirical or virtual) inter-hemispheric SC, this might indicate a fading interhemispheric communication and dynamical variability. The observation that inter-hemispheric SC decline decreases interhemispheric FCD variance in the virtual (VAB) characterization, as well as that lower inter-hemispheric SC is associated to lower interhemispheric FCD variance in the empirical data, suggests an emergence of functional dedifferentiation in older adults (Reuter-Lorenz and Park, 2014; Stumme et al., 2020). In line with aging theories, such as HAROLD or STAC, lower interhemispheric dynamics indicates higher recruitment of brain regions from both hemispheres and a consequently lower functional diversity or specialization (Battaglia et al., 2020; Lou et al., 2019). Both, higher bilateral recruitment and lower functional specialization might be reminiscent of reduced speed of reconfiguration possibilities of cognitive states (Lee et al., 2019; Power et al., 2011; Xia et al., 2019). Concurrently, the virtual framework presented a significantly higher coupling between SC and FCD, i.e. a higher global network parameter $G$, with higher age, but also with stronger SC deterioration (corrected for sex and education). Hence, this demonstrates that the global neuromodulation increases with age and with SC deterioration. While both sexes showed comparable correlations between G and age (supported by a non-significant interaction effect), females were found to exhibit lower modulation by SC on FC as compared to males within group comparisons. However, the role of sex and its interaction with age itself needs to be elucidated further in future studies, as it has been shown to be related to differences in structural and functional connectivity and potentially different trajectories of their reorganization during aging (Ficek-Tani et al., 2023; Ritchie et al., 2018; Sang et al., 2021).

Furthermore, we additionally related the BNMs to the heterogeneity of cognitive decline. Within this framework this was done by linearly relating cognitive performance to the modulation of $G$ (Reuter-Lorenz and Park, 2014). Here, we observed that a higher global $G$ was negatively related to verbal memory and concept shifting (Supplementary Table 1, Figs. 3 and 4). Lower performance in executive function as well as verbal memory has been repeatedly found to be particularly characteristic for cognitive decline in older adults (e.g. Reuter-Lorenz et al., 2021). For all other tests employed within the 1000BRAINS study no significant association was found. To further verify our observation of a negative relationship between higher $G$ and worse performance in executive functions, we additionally divided our sample in low versus high performing subjects. For executive function, we further observed that low performing subgroups showed a significantly higher $G$ as well as a stronger age-related increase in $G$ as compared to higher performing individuals. Given the age-related increase in SC-FC coupling is characterized by functional dedifferentiation, the slightly stronger age-related increase in $G$ in low performing individuals might additionally reflect an acceleration of these processes. Hence, this increased

SC-FC tethering might not only be associated with but even contribute to lower performance, and suggest an amplification of this loss of dynamical flexibility, especially in poor cognitive performers (Fig. 4). This may suggest a recalibration strategy due to Scaffolding for the first time, since the global modulation increase seems not to happen for the high performing group, likely due to better brain maintenance (Reuter-Lorenz and Park, 2014).

### 4.1. Limitations

We here focused particularly on the relation between differences in interhemispheric structural connectivity and functional connectivity dynamics, reflecting different brain modes of fluidity. The current study therefore exemplifies the aging process with one prominent example of aging-associated structural decline. In future studies it would be desirable to add additional processes as well as further influencing factors that might modify the aging process, such as sex, lifestyle choices or genetic differences. Further, regarding functional connectivity we chose to focus on positive correlations only, as often done in the literature since anti-correlations in resting-state data are not well understood yet. This could be investigated further in future model engineering studies. For future works, continuous analysis of the age trends could provide additional information beyond the median split of the group, as we have done here with the median age to get the general differences, assuming that the changes are monotonic, as indicated by reported trends.

Another possible limitation of this study is the identical form of the hemodynamic response function across brain regions and age that we have assumed, besides the fact that its variability confounds the analysis of resting-state fMRI (Rangaprakash et al., 2018). Moreover, the variability in BOLD signals during aging is explained not just by the neuronal activity, but also by the cerebrovascular and cardiovascular factors (Tsvetanov et al., 2021; West et al., 2019), with neuronal activity itself being also coupled to cardiovascular rhythms (Stankovski et al., 2016). As a result, BOLD hemodynamic function changes significantly with aging with its response becoming smoother (West et al., 2019), and this needs to be considered in further studies.

Our virtual brain framework covers only one part of the mechanisms which shape the brain's dynamics, that is the connectome. In absence of subject specific information, we have assumed identical parameters for each region, ignoring the known structural hierarchies (Wang et al., 2020), which have been shown to improve the predictive value of the brain network models (Chaudhuri et al., 2015; Schirner et al., 2018; Deco et al., 2021; Wang et al., 2023), even when the neuronal mass is implicit and data-driven (Sip et al., 2023). In that respect the lack of neuromodulation in our model prohibits testing the hypothesis about the dopaminergic nature of the global coupling parameter. In addition, this could be the reason for the different magnitudes of some of the observed values in the model, as compared with the empirical recordings. However, besides some first attempts (Kringelbach et al., 2020), the effect of neuromodulation in the brain network models is not as established as the effect of the connectivity (Breakspear 2017), even though averaged whole-brain maps of different receptors are now available (Hansen et al., 2022). In that sense our model can be considered as a first, more generic version, to be further customized to some of the distinct features of a given subject's brain beyond the connectome (Amunts et al., 2023).

## 5. Conclusion

The present study shows the first results from virtual aging models based on empirical data. Starting with the analysis of structural and functional age-related alterations, we identified the interhemispheric white-matter loss on the structural side and the interhemispheric fluidity and homotopic connectivity on the functional side. Then by manipulating the structure, trying to mimic the empirically observed trajectory of white-matter decline, we show that we observe the same trends in-silico for the aging trajectories, as well as for the simulated aging cohort. This is achieved under the assumption that the brain sets its working point at the maximal whole-brain fluidity. This is achieved through a gradual increase in the global coupling between the structure and the function, which we hypothesize to be of dopaminergic nature, and which would need to be verified with more detailed models.

The Bayesian SBI also confirms this increase of SC neuromodulation with aging on an individual basis and retrieves global modulation with the same age-declining FC and FCD features. This provides a causal validation of the VAB pipeline and suggests higher model evidence for higher $G$ values with age and thus a shift of the optimal working point of the brain with age. To our knowledge, besides being applied on a task-free paradigm, this is a direct evidence of scaffolding and dedifferentiation in aging leading to adverse effects of cognitive decline demonstrated within a subject-specific causal inference framework in a large cohort.

## Resource availability

Key resources table

| Reagent or resource | Source | Identifier |
|---|---|---|
| Deposited data | | |
| Structural connectivity data of the 1000 BRAINS dataset | EBRAINS | https://doi.org/10.25493%2F6640-3XH |
| Software or algorithms | | |
| The virtual aging brain | This paper | https://github.com/ins-amu/virtual_aging_brain |
| The virtual brain | The virtual brain foundation | https://github.com/the-virtual-brain/tvb-root https://www.thevirtualbrain.org/tvb/zwei/home |
| CAT12 toolbox | Structural Brain Mapping Group, University of Jena | http://www.neuro.uni-jena.de/cat/ |
| MRtrix | MRtrix | https://www.mrtrix.org/ |
| FSL (FMRIB Software Library) | Analysis Group, FMRIB, Oxford, UK | https://fsl.fmrib.ox.ac.uk/fsl/fslwiki/FSL |
| MCFLIRT, FLIRT, BET, SUSAN, ICA-AROMA | FSL (FMRIB Software Library) | |
| DVARS | Oxford Big Data Institute. | https://github.com/asoroosh/DVARS |

## Contact for reagents or resource sharing

Further information and requests for resources and reagents should be directed to and will be fulfilled by the lead contact Viktor Jirsa, viktor.jirsa@univ-amu.fr, and by the senior author Svenja Caspers, s.caspers@fz-juelich.de.

## Data and code availability

The code can be found in the following link (https://github.com/ins-amu/virtual_aging_brain). The code for the Virtual Brain is also public available at the following link (https://github.com/the-virtual-brain/tvb-root), while learning material to master the platform can be found at the TVB hub website (https://hub.thevirtualbrain.org/). The Structural Connectivity data are available on EBRAINS platform at the following DOI (https://doi.org/10.25493%2F6640-3XH), while the fMRI time series and the cognitive scores are available upon reasonable request by sending an email to the lead contact or to SC. After the creation of a personal account and the approval of its request, any EBRAINS user could download the data by accepting the EBRAINS data users agreement. The EBRAINS subscription works as an MTA between users and the data-owner. When a request for access to EBRAINS is done, any researcher can also find public implementation of various showcases that shows the variety of applications of TVB (https://ebrains.eu/service/the-virtual-brain/), such as an online showcase of the VAB that requires

no further installation on a personal machine (https://wiki.ebrains.eu/bin/view/Collabs/sga3-d1-2-showcase-1/).

## CRediT authorship contribution statement

**Mario Lavanga:** Conceptualization, Methodology, Investigation, Visualization, Software, Formal analysis, Writing – original draft. **Johanna Stumme:** Investigation, Visualization, Formal analysis, Writing – original draft. **Bahar Hazal Yalcinkaya:** Methodology, Software. **Jan Fousek:** Methodology, Investigation, Software. **Christiane Jockwitz:** Formal analysis. **Hiba Sheheitli:** Methodology. **Nora Bittner:** Formal analysis, Writing – review & editing. **Meysam Hashemi:** Methodology, Software, Writing – review & editing. **Spase Petkoski:** Methodology, Investigation, Writing – review & editing. **Svenja Caspers:** Conceptualization, Funding acquisition, Project administration, Supervision, Writing – original draft, Writing – review & editing. **Viktor Jirsa:** Conceptualization, Methodology, Funding acquisition, Project administration, Supervision, Writing – original draft, Writing – review & editing.

## Declaration of Competing Interest

The authors declare that they have no conflict of interest.

## Data availability

Data will be made available on request.

## Acknowledgments

This project was partially funded by the German National Cohort and the 1000BRAINS-Study of the Institute of Neuroscience and Medicine, Research Centre Jülich, Germany. We thank the Heinz Nixdorf Foundation (Germany) for the generous support of the Heinz Nixdorf Study. We thank the investigative group and the study staff of the Heinz Nixdorf Recall Study and 1000BRAINS. ML would like to thank Paul Triebkorn for the Visualization support and both Viktor Sip and Lionel Kusch for their insights on programming with HPC facilities. The authors also wish to acknowledge the financial support of the following agencies: the French National Research Agency (ANR) as part of the second “Investissements d’Avenir” program (ANR-17-RHUS-0004, EPINOV), European Union’s Horizon 2020 research and innovation program under grant agreement nos. 785907 (SGA2), and 945539 (SGA3) Human Brain Project, PHRC-I 2013 EPISODIUM (grant number 2014–27), the Fondation pour la Recherche Medicale (DIC20161236442), Virtual-BrainCloud (grant number 826421), the SATT Sud-Est (827-SA-16-UAM) for providing funding for this research project, the Initiative and Networking Fund of the Helmholtz Association (SC), the Psychiatric Imaging Network Germany (PING) project (BMBF 01 EE1405C).

## Supplementary materials

Supplementary material associated with this article can be found, in the online version, at doi:10.1016/j.neuroimage.2023.120403.

## References

Afyouni, S., Nichols, T.E., 2018. Insight and inference for DVARS. NeuroImage 172, 291–312. https://doi.org/10.1016/j.neuroimage.2017.12.098.

Amunts, K., Rowald, S., Sanchez-Vives, M.V., Axer, M., De Bonis, G., Salles, A., 2023. The coming decade of digital brain research—A vision for neuroscience at the intersection of technology and computing (No. FZJ-2022-01628). Zenodo. https://doi.org/10.5281/zenodo.7764003.

Andersson, J.L.R., Graham, M.S., Zsoldos, E., Sotiropoulos, S.N., 2016. Incorporating outlier detection and replacement into a non-parametric framework for movement and distortion correction of diffusion MR images. NeuroImage 141, 556–572. https://doi.org/10.1016/j.neuroimage.2016.06.058.

Ashburner, J., 2009. Computational anatomy with the SPM software. Magn. Reson. Imaging 27, 1163–1174. https://doi.org/10.1016/j.mri.2009.01.006.

Ashburner, J., Friston, K.J., 2005. Unified segmentation. NeuroImage 26, 839–851. https://doi.org/10.1016/j.neuroimage.2005.02.018.

Battaglia, D., Boudou, T., Hansen, E.C.A., Lombardo, D., Chettouf, S., Daffertshofer, A., McIntosh, A.R., Zimmermann, J., Ritter, P., Jirsa, V., 2020. Dynamic functional connectivity between order and randomness and its evolution across the human adult lifespan. NeuroImage 222, 117156. https://doi.org/10.1016/j.neuroimage.2020.117156.

Berry, A.S., Shah, V.D., Baker, S.L., Vogel, J.W., O’Neil, J.P., Janabi, M., Schwimmer, H. D., Marks, S.M., Jagust, W.J, 2016. Aging affects dopaminergic neural mechanisms of cognitive flexibility. J. Neurosci. 36, 12559–12569. https://doi.org/10.1523/JNEUROSCI.0626-16.2016.

Breakspear, M., 2017. Dynamic models of large-scale brain activity. Nat. Neurosci. 20 (3), 340–352.

Cabeza, R., 2002. Hemispheric asymmetry reduction in older adults: the HAROLD model. Psychol. Aging 17 (1), 85.

Cabeza, R., Anderson, N.D., Locantore, J.K., McIntosh, A.R., 2002. Aging gracefully: compensatory brain activity in high-performing older adults. NeuroImage 17 (3), 1394–1402.

Calhoun, V.D., Wager, T.D., Krishnan, A., Rosch, K.S., Seymour, K.E., Nebel, M.B., Mostofsky, S.H., Nyalakanai, P., Kiehl, K., 2017. The impact of T1 versus EPI spatial normalization templates for fMRI data analyses. Hum. Brain Mapp. 38, 5331–5342. https://doi.org/10.1002/hbm.23737.

Caspers, S., Moebus, S., Lux, S., Pundt, N., Schütz, H., Mühleisen, T.W., Gras, V., Eickhoff, S.B., Romanzetti, S., Stöcker, T., et al., 2014. Studying variability in human brain aging in a population-based German cohort—Rationale and design of 1000BRAINS. Front. Aging Neurosci. 6 https://doi.org/10.3389/fnagi.2014.00149.

Chaudhuri, R., Knoblauch, K., Gariel, M.A., Kennedy, H., Wang, X.J, 2015. A large-scale circuit mechanism for hierarchical dynamical processing in the primate cortex. Neuron 88 (2), 419–431. https://doi.org/10.1016/j.neuron.2015.09.008.

Cranmer, K., Brehmer, J., Louppe, G., 2020. The frontier of simulation-based inference. Proc. Natl. Acad. Sci 117, 30055–30062. https://doi.org/10.1073/pnas.1912789117.

Courtiol, J., Guye, M., Bartolomei, F., Petkoski, S., Jirsa, V.K., 2020. Dynamical mechanisms of interictal resting-state functional connectivity in epilepsy. J. Neurosci. 40 (29), 5572–5588.

Davis, S.W., Dennis, N.A., Daselaar, S.M., Fleck, M.S., Cabeza, R., 2008. Que PASA? The posterior–anterior shift in aging. Cereb. Cortex 18 (5), 1201–1209.

Davis, S.W., Kragel, J.E., Madden, D.J., Cabeza, R., 2012. The architecture of cross-hemispheric communication in the aging brain: linking behavior to functional and structural connectivity. Cereb. Cortex 22 (1), 232–242.

Damoiseaux, J.S., 2017. Effects of aging on functional and structural brain connectivity. NeuroImage 160, 32–40. https://doi.org/10.1016/j.neuroimage.2017.01.077.

Deco, G., Kringelbach, M.L., Arnatkeviciute, A., Oldham, S., Sabaroedin, K., Rogasch, N. C., Aquino, K.M., Fornito, A., 2021. Dynamical consequences of regional heterogeneity in the brain’s transcriptional landscape. Sci. Adv. 7 (29), eabf4752. https://doi.org/10.1126/sciadv.abf4752.

Dell’Acqua, F., Lacerda, L., Catani, M., Simmons, A., 2014. Anisotropic power maps: a diffusion contrast to reveal low anisotropy tissues from HARDI data. In: Proc Intl Soc Mag Reson Med, pp. 29960–29967.

Daselaar, S.M., Iyengar, V., Davis, S.W., Eklund, K., Hayes, S.M., Cabeza, R.E., 2015. Less wiring, more firing: low-performing older adults compensate for impaired white matter with greater neural activity. Cereb. Cortex 25 (4), 983–990.

Dohmatob, E., Varoquaux, G., Thirion, B., 2018. Inter-subject registration of functional images: do we need anatomical images? Front. Neurosci. 12.

Escrichs, A., Biarnes, C., Garre-Olmo, J., Fernández-Real, J.M., Ramos, R., Pamplona, R., Brugada, R., Serena, J., Ramió-Torrentà, L., Coll-De-Tuero, G., et al., 2021. Whole-brain dynamics in aging: disruptions in functional connectivity and the role of the rich club. Cereb. Cortex 31, 2466–2481. https://doi.org/10.1093/cercor/bhaa367.

Faskowitz, J., Esfahlani, F.Z., Jo, Y., Sporns, O., Betzel, R.F., 2020. Edge-centric functional network representations of human cerebral cortex reveal overlapping system-level architecture. Nat. Neurosci. 23, 1644–1654. https://doi.org/10.1038/s41593-020-00719-y.

Festini, S.B., Zahodne, L., and Reuter-Lorenz, P.A. (2018). Theoretical Perspectives on Age Differences in Brain Activation: HAROLD, PASA, CRUNCH—How Do They STAC Up?.

Ficek-Tani, B., Horien, C., Ju, S., Xu, W., Li, N., Lacadie, C., Fredericks, C., 2023. Sex differences in default mode network connectivity in healthy aging adults. Cereb. Cortex 33 (10), 6139–6151.

Friston, K.J., Mechelli, A., Turner, R., Price, C.J., 2000. Nonlinear responses in fMRI: the Balloon model, Volterra kernels, and other hemodynamics. NeuroImage 12, 466–477. https://doi.org/10.1006/nimg.2000.0630.

Fousek, J., Rabuffo, G., Gudibanda, K., Sheheitli, H., Jirsa, V., & Petkoski, S. (2022). Symmetry breaking organizes the brain’s resting state manifold. bioRxiv, 2022-01. doi: https://doi.org/10.1101/2022.01.03.474841.

Gaser, C., Dahnke, R., Thompson, P.M., Kurth, F., Luders, E., Alzheimer’s Disease Neuroimaging Initiative, 2022. CAT–A computational anatomy toolbox for the analysis of structural MRI data. biorxiv. https://doi.org/10.1101/2022.06.11.495736.

Gonçalves, P.J., Lueckmann, J.-M., Deistler, M., Nonnenmacher, M., Öcal, K., Bassetto, G., Chintaluri, C., Podlaski, W.F., Haddad, S.A., Vogels, T.P., et al., 2020. Training deep neural density estimators to identify mechanistic models of neural dynamics. Elife 9, e56261. https://doi.org/10.7554/eLife.56261.

Hashemi, M., Vattikonda, A.N., Jha, J., Sip, V., Woodman, M.M., Bartolomei, F., Jirsa, V. K., 2023. Amortized Bayesian inference on generative dynamical network models of epilepsy using deep neural density estimators. Neural Netw. 163, 178–194.
Hashemi, M., Vattikonda, A.N., Sip, V., Guye, M., Bartolomei, F., Woodman, M.M., Jirsa, V.K., 2020. The Bayesian virtual epileptic patient: a probabilistic framework designed to infer the spatial map of epileptogenicity in a personalized large-scale brain model of epilepsy spread. NeuroImage 217, 116839.
Hashemi, M., Vattikonda, A.N., Sip, V., Diaz-Pier, S., Peyser, A., Wang, H., Guye, M., Bartolomei, F., Woodman, M.M., Jirsa, V.K., 2021. On the influence of prior information evaluated by fully Bayesian criteria in a personalized whole-brain model of epilepsy spread. PLoS Comput. Biol. 17 (7), e1009129.
Hansen, J.Y., Shafiei, G., Markello, R.D., Smart, K., Cox, S.M., Nørgaard, M., Misic, B., 2022. Mapping neurotransmitter systems to the structural and functional organization of the human neocortex. Nat. Neurosci. 25, 1569–1581.
Hedden, T., Gabrieli, J.D.E., 2004. Insights into the ageing mind: a view from cognitive neuroscience. Nat. Rev. Neurosci. 5, 87–96. https://doi.org/10.1038/nrn1323.
Jeurissen, B., Tournier, J.-D., Dhollander, T., Connelly, A., Sijbers, J., 2014. Multi-tissue constrained spherical deconvolution for improved analysis of multi-shell diffusion MRI data. NeuroImage 103, 411–426. https://doi.org/10.1016/j.neuroimage.2014.07.061.
Kringelbach, M.L., Cruzat, J., Cabral, J., Knudsen, G.M., Carhart-Harris, R., Whybrow, P. C., Logothetis, N.K., Deco, G., 2020. Dynamic coupling of whole-brain neuronal and neurotransmitter systems. Proc. Natl. Acad. Sci. 117 (17), 9566–9576.
Lee, H., Golkowski, D., Jordan, D., Berger, S., Ilg, R., Lee, J., Mashour, G.A., Lee, U., Avidan, M.S., Blain-Moraes, S., et al., 2019. Relationship of critical dynamics, functional connectivity, and states of consciousness in large-scale human brain networks. NeuroImage 188, 228–238. https://doi.org/10.1016/j.neuroimage.2018.12.011.
Lou, W., Wang, D., Wong, A., Chu, W.C.W., Mok, V.C.T., Shi, L., 2019. Frequency-specific age-related decreased brain network diversity in cognitively healthy elderly: a whole-brain data-driven analysis. Hum. Brain Mapp. 40, 340–351. https://doi.org/10.1002/hbm.24376.
Lurie, D.J., Kessler, D., Bassett, D.S., Betzel, R.F., Breakspear, M., Kheilholz, S., Kucyi, A., Liégeois, R., Lindquist, M.A., McIntosh, A.R., et al., 2020. Questions and controversies in the study of time-varying functional connectivity in resting fMRI. Netw. Neurosci. 4, 30–69. https://doi.org/10.1162/netn_a_00116.
Malagurski, B., Liem, F., Oschwald, J., Mérillat, S., Jäncke, L., 2020. Functional dedifferentiation of associative resting state networks in older adults–a longitudinal study. NeuroImage 214, 116680.
Mollink, J., Smith, S.M., Elliott, L.T., Kleinnijenhuis, M., Hiemstra, M., Alfaro-Almagro, F., Marchini, J., van Cappellen van Walsum, A.-M., Jbabdi, S., Miller, K.L., 2019. The spatial correspondence and genetic influence of interhemispheric connectivity with white matter microstructure. Nat. Neurosci. 22, 809–819. https://doi.org/10.1038/s41593-019-0379-2.
Montbrió, E., Pazó, D., Roxin, A., 2015. Macroscopic description for networks of spiking neurons. Phys. Rev. X 5, 021028. https://doi.org/10.1103/PhysRevX.5.021028.
Naik, S., Banerjee, A., Bapi, R.S., Deco, G., Roy, D, 2017. Metastability in senescence. Trends Cogn. Sci. 21, 509–521. https://doi.org/10.1016/j.tics.2017.04.007.
Papamakarios, G., Pavlakou, T., Murray, I., 2017. Masked autoregressive flow for density estimation. Adv. Neural Inf. Process. Syst. 30.
Park, D.C., Polk, T.A., Park, R., Minear, M., Savage, A., Smith, M.R., 2004. Aging reduces neural specialization in ventral visual cortex. Proc. Natl. Acad. Sci. 101 (35), 13091–13095.
Parkes, L., Fulcher, B., Yücel, M., Fornito, A., 2018. An evaluation of the efficacy, reliability, and sensitivity of motion correction strategies for resting-state functional MRI. NeuroImage 171, 415–436. https://doi.org/10.1016/j.neuroimage.2017.12.073.
Pathak, A., Sharma, V., Roy, D., Banerjee, A., 2022. Biophysical mechanism underlying compensatory preservation of neural synchrony over the adult lifespan. Commun. Biol. 5 (1), 567.
Petkoski, S., Jirsa, V.K., 2019. Transmission time delays organize the brain network synchronization. Philos. Trans. R. Soc. A 377 (2153), 20180132.
Petkoski, S., Jirsa, V.K., 2022. Normalizing the brain connectome for communication through synchronization. Netw. Neurosci. 6 (3), 722–744.
Petkoski, S., Ritter, P., Jirsa, V.K., 2023. White-matter degradation and dynamical compensation support age-related functional alterations in human brain. Cereb. Cortex 33 (10), 6241–6256.
Power, J.D., Cohen, A.L., Nelson, S.M., Wig, G.S., Barnes, K.A., Church, J.A., Vogel, A.C., Laumann, T.O., Miezin, F.M., Schlaggar, B.L., et al., 2011. Functional network organization of the human brain. Neuron 72, 665–678. https://doi.org/10.1016/j.neuron.2011.09.006.
Pruim, R.H.R., Mennes, M., Buitelaar, J.K., Beckmann, C.F., 2015. Evaluation of ICA-AROMA and alternative strategies for motion artifact removal in resting state fMRI. NeuroImage 112, 278–287. https://doi.org/10.1016/j.neuroimage.2015.02.063.
Puxeddu, M.G., Faskowitz, J., Betzel, R.F., Petti, M., Astolfi, L., Sporns, O., 2020. The modular organization of brain cortical connectivity across the human lifespan. NeuroImage 218, 116974. https://doi.org/10.1016/j.neuroimage.2020.116974.
Rabuffo, G., Fousek, J., Bernard, C., Jirsa, V., 2021. Neuronal cascades shape whole-brain functional dynamics at rest. eNeuro 8. https://doi.org/10.1523/ENEURO.0283-21.2021.
Rangaprakash, D., Wu, G.R., Marinazzo, D., Hu, X., Deshpande, G., 2018. Hemodynamic response function (HRF) variability confounds resting-state fMRI functional connectivity. Magn. Reson. Med. 80 (4), 1697–1713.
Reuter-Lorenz, P.A., Cappell, K.A., 2008. Neurocognitive aging and the compensation hypothesis. Curr. Dir. Psychol. Sci. 17 (3), 177–182.
Reuter-Lorenz, P.A., Festini, S.B., Jantz, T.K., 2021. Executive functions and neurocognitive aging. In: *Handbook of the Psychology of Aging*. Academic Press, pp. 67–81.
Reuter-Lorenz, P.A., Park, D.C., 2014. How does it STAC up? Revisiting the scaffolding theory of aging and cognition. Neuropsychol. Rev. 24, 355–370. https://doi.org/10.1007/s11065-014-9270-9.
Ritchie, S.J., Cox, S.R., Shen, X., Lombardo, M.V., Reus, L.M., Alloza, C., Deary, I.J., 2018. Sex differences in the adult human brain: evidence from 5216 UK biobank participants. Cereb. Cortex 28 (8), 2959–2975.
Roland, J.L., Snyder, A.Z., Hacker, C.D., Mitra, A., Shimony, J.S., Limbrick, D.D., Raichle, M.E., Smyth, M.D., Leuthardt, E.C., 2017. On the role of the corpus callosum in interhemispheric functional connectivity in humans. Proc. Natl. Acad. Sci 114, 13278–13283. https://doi.org/10.1073/pnas.1707050114.
Sang, F., Chen, Y., Chen, K., Dang, M., Gao, S., Zhang, Z., 2021. Sex differences in cortical morphometry and white matter microstructure during brain aging and their relationships to cognition. Cereb. Cortex 31 (11), 5253–5262.
Sanz Leon, P., Knock, S.A., Woodman, M.M., Domide, L., Mersmann, J., McIntosh, A.R., Jirsa, V., 2013. The virtual brain: a simulator of primate brain network dynamics. Front. Neuroinform. 7 https://doi.org/10.3389/fninf.2013.00010.
Schaefer, A., Kong, R., Gordon, E.M., Laumann, T.O., Zuo, X.-N., Holmes, A.J., Eickhoff, S.B., Yeo, B.T.T., 2018. Local-global parcellation of the human cerebral cortex from intrinsic functional connectivity MRI. Cereb. Cortex 28, 3095–3114. https://doi.org/10.1093/cercor/bhx179.
Schirner, M., McIntosh, A.R., Jirsa, V., Deco, G., Ritter, P., 2018. Inferring multi-scale neural mechanisms with brain network modelling. Elife 7, e28927.
Schirner, M., Domide, L., Perdikis, D., Triebkorn, P., Stefanovski, L., Pai, R., Ritter, P., 2022. Brain simulation as a cloud service: the virtual brain on EBRAINS. NeuroImage 251, 118973.
Senden, M., Reuter, N., van den Heuvel, M.P., Goebel, R., Deco, G., 2017. Cortical rich club regions can organize state-dependent functional network formation by engaging in oscillatory behavior. NeuroImage 146, 561–574. https://doi.org/10.1016/j.neuroimage.2016.10.044.
Sip, V., Hashemi, M., Dickscheid, T., Amunts, K., Petkoski, S., Jirsa, V., 2023. Characterization of regional differences in resting-state fMRI with a data-driven network model of brain dynamics. Sci. Adv. 9 (11), eabq7547.
Smith, R.E., Tournier, J.-D., Calamante, F., Connelly, A., 2015. The effects of SIFT on the reproducibility and biological accuracy of the structural connectome. NeuroImage 104, 253–265. https://doi.org/10.1016/j.neuroimage.2014.10.004.
Stankovski, T., Petkoski, S., Raeder, J., Smith, A.F., McClintock, P.V., Stefanovska, A., 2016. Alterations in the coupling functions between cortical and cardio-respiratory oscillations due to anaesthesia with propofol and sevoflurane. Philos. Trans. R. Soc. A 374 (2067), 20150186.
Stumme, J., Jockwitz, C., Hoffstaedter, F., Amunts, K., Caspers, S., 2020. Functional network reorganization in older adults: graph-theoretical analyses of age, cognition and sex. NeuroImage 214, 116756. https://doi.org/10.1016/j.neuroimage.2020.116756.
Tournier, J.-D., Calamante, F., Connelly, A., 2012. MRtrix: diffusion tractography in crossing fiber regions. Int. J. Imaging Syst. Technol. 22, 53–66. https://doi.org/10.1002/ima.22005.
Tsvetanov, K.A., Henson, R.N., Jones, P.S., Mutsaerts, H., Fuhrmann, D., Tyler, L.K., Rowe, J.B., 2021. The effects of age on resting-state BOLD signal variability is explained by cardiovascular and cerebrovascular factors. Psychophysiology 58 (7), e13714.
Wang, X.J., 2020. Macroscopic gradients of synaptic excitation and inhibition in the neocortex. Nature Rev. Neurosci. 21 (3), 169–178.
Wang, H.E., Woodman, M., Triebkorn, P., Lemarechal, J.D., Jha, J., Dollomaja, B., Vattikonda, A.N., Sip, V., Medina Villalon, S., Hashemi, M., Guye, M., 2023. Delineating epileptogenic networks using brain imaging data and personalized modeling in drug-resistant epilepsy. Sci. Transl. Med. 15 (680), eabp8982.
Wells, W.M., Viola, P., Atsumi, H., Nakajima, S., Kikinis, R., 1996. Multi-modal volume registration by maximization of mutual information. Med. Image Anal. 1, 35–51. https://doi.org/10.1016/S1361-8415(01)80004-9.
West, K.L., Zuppichini, M.D., Turner, M.P., Sivakolundu, D.K., Zhao, Y., Abdelkarim, D., Rypma, B., 2019. BOLD hemodynamic response function changes significantly with healthy aging. NeuroImage 188, 198–207.
Xia, Y., Chen, Q., Shi, L., Li, M., Gong, W., Chen, H., Qiu, J., 2019. Tracking the dynamic functional connectivity structure of the human brain across the adult lifespan. Hum. Brain Mapp. 40, 717–728. https://doi.org/10.1002/hbm.24385.
Zimmermann, J., Ritter, P., Shen, K., Rothmeier, S., Schirner, M., McIntosh, A.R., 2016. Structural architecture supports functional organization in the human aging brain at a regionwise and network level: structure supports function in aging. Hum. Brain Mapp. 37, 2645–2661. https://doi.org/10.1002/hbm.23200.
Zhang, H., Lee, A., Qiu, A., 2017. A posterior-to-anterior shift of brain functional dynamics in aging. Brain Struct. Funct. 222, 3665–3676.
Zuo, X.-N., Kelly, C., Martino, A.D., Mennes, M., Margulies, D.S., Bangaru, S., Grzadzinski, R., Evans, A.C., Zang, Y.-F., Castellanos, F.X., et al., 2010. Growing together and growing apart: regional and sex differences in the lifespan developmental trajectories of functional homotopy. J. Neurosci. 30, 15034–15043. https://doi.org/10.1523/JNEUROSCI.2612-10.2010.